Statistical properties of an incompressible passive vector convected by isotropic turbulence

Jingyuan Yang,[1] Toshiyuki Gotoh,[1,*] Hideaki Miura,[2] and Takeshi Watanabe[1]
[1]*Department of Physical Science and Engineering, Nagoya Institute of Technology, Gokiso, Nagoya 466-8555, Japan*
[2]*National Institute for Fusion Science, Oroshi, Toki City, Gifu 509-5292, Japan*

(Received 25 January 2019; published 3 June 2019)

Statistical properties of an incompressible passive vector convected by homogeneous isotropic turbulence are studied by comparing to the velocity and passive scalar, in order to explore the physics behind the differences and similarities in the statistical properties between the velocity vector and passive scalar. The passive vector obeys an equation similar to the Navier-Stokes equation, with a pseudopressure to ensure the incompressibility of the vector. The von Kármán–Howarth equation for the passive vector is derived and the average of the velocity increment times the square of the passive vector increments obeys a 4/3 law in the inertial-convective range. We carried out direct numerical simulations (DNSs) of up to 1024^3 grid points. The spectra of the kinetic and pseudokinetic energies and the scalar variance obey a $k^{-5/3}$ power law. The Kolmogorov constants are $C_K = 1.57$ for the velocity and $C_K^w = 0.99$ for the passive vector, and the Obukhov-Corrsin constant of the passive scalar is $C_{OC} = 0.67$. The spectral bump of the compensated spectrum of the passive vector is slightly larger than that of the velocity, but smaller than the passive scalar. It is found that the behavior of the passive vector fluctuations at large scales is close to that of the velocity due to the nonlocal effects of the pseudo-pressure, while the small-scale fluctuations resemble those of the passive scalar. The nonlinearity of the convective term is key to the differences between the velocity and passive fields at small scales.

DOI: 10.1103/PhysRevFluids.4.064601

I. INTRODUCTION

In addition to turbulence itself, problems of scalar mixing by turbulent flow are one of the central issues in the fundamental physics of turbulence [1]. Scalars that do not react to a fluid are called passive scalars, and their behavior is considered to be a canonical problem in turbulence research [2]. The Kolmogorov theory of turbulence [3] has been used to derive the Obukhov-Corrsin spectrum of the scalar variance [4,5] and the Yaglom 4/3 law for the cubic moments of the velocity increment times the squared scalar increment [6]. The scalar spectra of the various Schmidt numbers have been determined in the inertial-diffusive and viscous-convective ranges at low and high Schmidt numbers, respectively [7,8].

Although the statistics of the scalar at low order moments are similar to those of the velocity, it is widely recognized that in the inertial-convective range the scaling exponents of the moments of the passive scalar increment at high order are smaller than those of the velocity and tend to saturate, meaning that the passive scalar is more intermittent than the velocity field [9–12], and that the spatial structure of large scalar gradients is sheet-like, in contrast to the vortex tubes of the

*gotoh.toshiyuki@nitech.ac.jp

velocity [11,13–15]. Kraichnan proposed a model for the passive scalar known as the Kraichnan model [16,17]. In the model, the velocity field is assumed to follow a Gaussian distribution with a delta correlation in time (Kraichnan velocity ensemble [18]). The most novel aspect of the model is that the scaling exponents of the moments of the scalar increments can be derived analytically. Since then, there have been extensive studies regarding the scaling exponents. The scaling exponents of the moments in the model are determined by the zero mode of the linear operator for the scalar moments and are thus universal [19,20].

Celani *et al.* [21] studied the passive scalar and active scalar in two-dimensional convective turbulence and argued that the statistical nature of the velocity increments is close to Gaussian, self similar, and universal with respect to the forcing mechanisms in the inverse cascading range, and also found that the statistical properties of the active (temperature) and passive scalars are the same and thus universal with respect to the scalar injection mechanisms [9,21–24]. The above facts seem to suggest that a mechanism analogous to the zero mode of some operator could be applied to the the passive scalar fluctuations convected by the Navier-Stokes turbulent flow in the forward cascading range, and thus the passive scalar statistics is universal. However, the turbulent velocity field in three dimensions obeying the Navier-Stokes equation differs significantly from the Kraichnan velocity ensemble, being neither Gaussian nor white noise, and the energy is forward cascading. Indeed, Gotoh and Watanabe [25] studied the intermittency of two passive scalars in three dimensions that are convected by the same turbulent velocity field of the Navier-Stokes equation, but are excited by different mechanisms, one being the uniform mean gradient and the other being Gaussian white random injection. Remarkably, it was found that the scaling exponents of the moments of the scalar increments differ at large scales, and are thus not universal [25].

The above observations and various data from experiments and numerical simulations suggest that the passive scalar fluctuations are not as universal as in the velocity, and that our understanding of the universality of the passive scalar fluctuations is still not enough. Then it is natural to explore the physics which generates the differences in the statistical properties between the velocity and the passive scalar, instead of studying the intrinsic behavior of the passive scalar fluctuations, such as scaling exponents, probability distribution functions (PDFs) and so on. This is our starting motivation.

One may think that the differences arise from the existence of the pressure term. The pressure prevents a fluid blob from being indefinitely compressed in the absence of viscosity, while there is no restriction on the passive scalar, and the scalar gradient can grow indefinitely until it balances the diffusive action. It is, therefore, reasonable to consider that the pressure suppresses the intermittency; as Kraichnan pointed out, pressure is an intermittency killer [26,27]. However, we do not know the extent to which the pressure suppresses the buildup of the intermittency as the scale decreases. There is another point to consider: whether the equation is linear or nonlinear. Since the pressure and nonlinearity are complexly interwoven through the nonlocal kernel, it is not certain whether or not two factors could be separately examined.

One way to get insight into the problem is to introduce an artificial vector field, i.e., an incompressible passive vector convected by turbulence, say $\boldsymbol{w}$, that has an intermediate property between the velocity and the passive scalar, and to investigate its properties by comparing them to those of the velocity and passive scalar. Our hope is that the introduction of $\boldsymbol{w}$ may make comparison easier and provide hints toward obtaining deeper understanding of the roles of incompressibility and pressure in turbulent flow, and their differences and similarities.

This is not the first time that passive vectors have been investigated. Yoshida and Kaneda [28] considered an incompressible passive vector given by

$$\left(\frac{\partial}{\partial t}+\boldsymbol{u}\cdot\nabla\right)\boldsymbol{w}=\ -\gamma_1\nabla q+\gamma_2\boldsymbol{w}\cdot\nabla\boldsymbol{u}+\alpha\nabla^2\boldsymbol{u}, \tag{1}$$

$$\nabla\cdot\boldsymbol{w}=0, \tag{2}$$

where γ_1 and γ_2 are nondimensional constants. When $(\gamma_1, \gamma_2) = (0, 1)$, the equation describes the evolution of the passive magnetic field, in which case the magnetic field $\boldsymbol{w}$ is excited through the second term of the right-hand side of Eq. (1). The equation for $(\gamma_1, \gamma_2) = (1, -1)$ becomes the linearized equation for small disturbances to the basic flow $\boldsymbol{u}$, and the disturbance $\boldsymbol{w}$ is excited by the basic flow. The equation for $(\gamma_1, \gamma_2) = (1, 0)$ is of peculiar importance in the present study because of physical properties described later.

Yoshida and Kaneda [28] studied the anomalous scaling of the anisotropy of second-order moments of the passive vector for the Kraichnan velocity ensemble in two dimensions. They showed analytically that the exponent of the isotropic sector is independent of the existence of a pressure-like term, while the anisotropic sector depends on whether the pressure-like term is present. Adzhemyan *et al.* [18] studied the case of $(\gamma_1, \gamma_2) = (1, \gamma_2)$ for the Kraichnan velocity ensemble in d dimensions through renormalization group (RG) analysis. When $\gamma_2 = 0$ the normal scaling is present. Ohkitani [29] used direct numerical simulation (DNS) to investigate the passive magnetic vector and investigated the effects of the Biot-Savart law and the reduction of the nonlinearity. They found that the magnetohydrodynamics (MHD) type passive vector tends to be more stretched than the velocity over short timescales. Benzi, Biferale, and Toschi [30] studied the statistical properties of the fluxes of solenoidal passive vectors and found that they are the same as those of the turbulent velocity. They also investigated scaling exponents by integrating the shell model of the passive scalar, and found that they are equal to those of the velocity shell model. Ching, Cohen, Gilbert, and Procaccia [31] carried out simulations with shell models for passive vectors and active vectors, and found that the scaling exponents of the structure functions are dominated by the zero modes, regardless of whether or not they are passive. Antonov and his coworkers studied anomalous scaling of solenoidal passive vectors convected by Gaussian random velocity with finite correlations in time using the renormalization group theory [32–34]. They investigated the universality of the exponents, their dependence on or independence of forcing, and effects of large-scale anisotropy, compressibility, and pressure.

The equation for $(\gamma_1, \gamma_2) = (1, 0)$ has features in common with the Navier-Stokes equation, such as

(1) three components in $\boldsymbol{w}$,
(2) the convection by the velocity $\boldsymbol{u}$,
(3) the pseudopressure q and incompressibility of $\boldsymbol{w}$,
(4) the pseudoviscosity α,
(5) when α is absent, the total pseudoenergy $(1/2) \int \boldsymbol{w}^2 d\boldsymbol{x}$ is conserved;

the difference is the fact that the convective term is linear.

When compared to the passive scalar, the common properties of the equation of $\boldsymbol{w}$ are

(1) the linearity of the convective term,
(2) the molecular dissipation.

The difference is the fact that three components of $\boldsymbol{w}$ are constrained through the incompressibility while the passive scaler is free from constraints.

Since our purpose is to explore the physics behind the differences and similarities between the velocity and passive scalar, the above properties of the passive vector $\boldsymbol{w}$ with $(\gamma_1, \gamma_2) = (1, 0)$ provide a convenient basis for comparing the passive vector to the velocity and passive scalar. Although there are some studies about this type of passive vector, comprehensive data ares not available. In order to obtain an overall picture of the incompressible passive vector, it is important to obtain detailed data from low to high order statistics. In the present paper, we compare the fundamental data of the second and third order statistics of the velocity, passive vector, and passive scalar, and examine them from the viewpoints of similarity and difference. The high order statistics and intermittency of three fields will be examined in a separate paper [35].

The paper is organized as follows. The governing equations are described in Sec. II. The theory of passive vector fluctuations is described under the assumptions of statistical homogeneity and isotropy in Sec. III. The settings and parameters used in the DNSs of the passive scalar are defined

in Sec. IV. The results of the DNS are presented in Sec. V and discussed in Sec. VI. We summarize the paper in Sec. VII.

II. GOVERNING EQUATIONS

We consider a passive scalar $\theta(\boldsymbol{x}, t)$ and a solenoidal passive vector $\boldsymbol{w}(\boldsymbol{x}, t)$, which are convected by the turbulent velocity $\boldsymbol{u}(\boldsymbol{x}, t)$ of an incompressible fluid with unit density under periodic boundary conditions. These are assumed to be governed by the following equations:

$$\left(\frac{\partial}{\partial t} + \boldsymbol{u}\cdot\nabla\right)\boldsymbol{u} = -\nabla p + \nu\nabla^2\boldsymbol{u}, \tag{3}$$

$$\nabla\cdot\boldsymbol{u} = 0, \tag{4}$$

$$\left(\frac{\partial}{\partial t} + \boldsymbol{u}\cdot\nabla\right)\boldsymbol{w} = -\nabla q + \alpha\nabla^2\boldsymbol{w}, \tag{5}$$

$$\nabla\cdot\boldsymbol{w} = 0, \tag{6}$$

$$\left(\frac{\partial}{\partial t} + \boldsymbol{u}\cdot\nabla\right)\theta = \kappa\nabla^2\theta, \tag{7}$$

where $p(\boldsymbol{x}, t)$ is the pressure, $q(\boldsymbol{x}, t)$ is called the pseudopressure in this paper, ν denotes the kinetic viscosity, α the pseudoviscosity of $\boldsymbol{w}$, and κ the diffusive coefficient for θ.

Under the incompressibility and periodic boundary conditions, the convective pressure and pseudopressure terms conserve the kinetic energy:

$$\int u_i\partial_j(u_iu_j + p\delta_{ij})\,dV = \int\left(\frac{1}{2}|\boldsymbol{u}|^2 + p\right)u_jn_j dS = 0, \tag{8}$$

$$\int w_i\partial_j(w_iu_j + q\delta_{ij})\,dV = \int\left(\frac{1}{2}|\boldsymbol{w}|^2 + q\right)u_jn_j dS = 0, \tag{9}$$

$$\int \theta\partial_j(\theta u_j)\,dV = \int\frac{1}{2}\theta^2u_jn_j dS = 0, \tag{10}$$

where $\boldsymbol{n}$ is the unit normal vector on the surface and we assume the summation convention for repeated indices. Therefore, in the absence of external forces and sources, we obtain the following equations:

$$\frac{d}{dt}\int\frac{1}{2}\boldsymbol{u}^2dV = -\nu\int(\nabla\boldsymbol{u})^2dV = -\epsilon_{\text{total}} \tag{11}$$

$$\frac{d}{dt}\int\frac{1}{2}\boldsymbol{w}^2dV = -\alpha\int(\nabla\boldsymbol{w})^2dV = -\epsilon^w_{\text{total}}, \tag{12}$$

$$\frac{d}{dt}\int\frac{1}{2}\theta^2dV = -\kappa\int(\nabla\theta)^2dV = -\chi_{\text{total}}, \tag{13}$$

where ϵ_{total}, $\epsilon^w_{\text{total}}$, and χ_{total} denote the dissipation rates of the total kinetic energy, total pseudokinetic energy, and total passive scalar variance per unit mass, respectively.

III. THEORY

We first consider the exact and fundamental statistical properties derived from the above equations. Under the homogeneous and isotropic assumptions, we define the following correlation functions:

$$u_0^2f^u(r) = \langle u_L(\boldsymbol{x})u_L(\boldsymbol{x}+\boldsymbol{r})\rangle, \tag{14}$$

$$w_0^2 f^w(r) = \langle w_L(\boldsymbol{x}) w_L(\boldsymbol{x}+\boldsymbol{r})\rangle, \tag{15}$$

$$\theta_0^2 f^\theta(r) = \langle \theta(\boldsymbol{x})\theta(\boldsymbol{x}+\boldsymbol{r})\rangle, \tag{16}$$

$$u_0^3 h^{uuu}(r) = \langle u_L(\boldsymbol{x}) u_L(\boldsymbol{x}) u_L(\boldsymbol{x}+\boldsymbol{r})\rangle, \tag{17}$$

$$u_0 w_0^2 h^{uww}(r) = \langle u_L(\boldsymbol{x}) w_L(\boldsymbol{x}) w_L(\boldsymbol{x}+\boldsymbol{r})\rangle, \tag{18}$$

$$u_0 w_0^2 q^{uww}(r) = \langle u_L(\boldsymbol{x}) w_T(\boldsymbol{x}) w_T(\boldsymbol{x}+\boldsymbol{r})\rangle, \tag{19}$$

$$u_0 \theta_0^2 h^{u\theta\theta}(r) = \langle u_L(\boldsymbol{x}) \theta(\boldsymbol{x}) \theta(\boldsymbol{x}+\boldsymbol{r})\rangle, \tag{20}$$

where $\langle\ \rangle$ denotes the ensemble average, u_0, w_0, and θ_0 are the root-mean-square values of $\boldsymbol{u}$, $\boldsymbol{w}$, and θ, respectively, u_L and w_L are the longitudinal components of $\boldsymbol{u}$ and $\boldsymbol{w}$ along the separation vector $\boldsymbol{r}$, respectively, and w_T denotes the transverse component of $\boldsymbol{w}$. Then, by using standard algebra we can obtain the von Kármán–Howarth equations

$$\frac{\partial}{\partial t} u_0^2 f^u(r) = \left(\frac{\partial}{\partial r} + \frac{4}{r}\right) u_0^3 h^{uuu}(r) + 2\nu \left(\frac{\partial^2}{\partial r^2} + \frac{4}{r}\frac{\partial}{\partial r}\right) u_0^2 f^u(r) \tag{21}$$

for the velocity,

$$\frac{\partial}{\partial t} w_0^2 f^w(r) = \frac{2}{r} u_0 w_0^2 [h^{uww}(r) + 2q^{uww}(r)] + 2\alpha \left(\frac{\partial^2}{\partial r^2} + \frac{4}{r}\frac{\partial}{\partial r}\right) w_0^2 f^w(r) \tag{22}$$

for the passive vector, and

$$\frac{\partial}{\partial t} \theta_0^2 f^\theta(r) = 2u_0 \theta_0^2 \left(\frac{\partial}{\partial r} + \frac{2}{r}\right) h^{u\theta\theta}(r) + 2\kappa \left(\frac{\partial^2}{\partial r^2} + \frac{2}{r}\frac{\partial}{\partial r}\right) \theta_0^2 f^\theta(r), \tag{23}$$

for the passive scalar.

Equations (21), (22), and (23) can be rewritten in terms of the increments of the velocity, passive vector, and passive scalar, as follows:

$$\delta u_L(\boldsymbol{x}, \boldsymbol{r}) = u_L(\boldsymbol{x}+\boldsymbol{r}) - u_L(\boldsymbol{x}), \tag{24}$$

$$\delta\theta(\boldsymbol{x}, \boldsymbol{r}) = \theta(\boldsymbol{x}+\boldsymbol{r}) - \theta(\boldsymbol{x}), \tag{25}$$

$$\delta \boldsymbol{w}(\boldsymbol{x}, \boldsymbol{r}) = \boldsymbol{w}(\boldsymbol{x}+\boldsymbol{r}) - \boldsymbol{w}(\boldsymbol{x}), \tag{26}$$

When the Reynolds and Péclet numbers are large, we expect there to be inertial and inertial convective ranges in which neither external excitations at large scales nor molecular dissipation are relevant to the dynamics. Thus, we can obtain Kolmogorov's 4/5 law

$$-\tfrac{4}{5}\bar{\epsilon} r = \langle (\delta u_L)^3 \rangle \tag{27}$$

for the velocity, Yaglom's 4/3 law

$$-\tfrac{4}{3}\bar{\chi} r = \langle (\delta u_L)(\delta\theta)^2 \rangle \tag{28}$$

for the passive scalar, and a new 4/3 law

$$-\tfrac{4}{3}\bar{\epsilon}_w r = \langle (\delta u_L)|\delta \boldsymbol{w}|^2 \rangle \tag{29}$$

for the passive vector, where $\bar{\epsilon}$, $\bar{\epsilon}_w$, and $\bar{\chi}$ are defined as

$$\bar{\epsilon} = \nu\langle(\nabla \boldsymbol{u})^2\rangle,\ \ \bar{\epsilon}_w = \alpha\langle(\nabla \boldsymbol{w})^2\rangle,\ \ \bar{\chi} = \kappa\langle(\nabla\theta)^2\rangle. \tag{30}$$

It should be noted that when $\mathrm{Sc}_\alpha \equiv \nu/\alpha$ is large the 4/3 law for the passive vector Eq. (29) holds also in the viscous-convective range [1].

A. Spectral analysis and Kolmogorov-Obukhov-Corrsin scaling

In a periodic cubic box with volume $V = L_{\mathrm{Box}}^3$, any fields $A(\boldsymbol{x}, t)$ can be expanded in terms of the Fourier series, as follows:

$$A(\boldsymbol{x}, t) = \sum_{\boldsymbol{k}} A(\boldsymbol{k}, t) e^{\mathrm{i}\boldsymbol{k}\cdot\boldsymbol{x}}, \tag{31}$$

$$A(\boldsymbol{k}, t) = \frac{1}{V} \int A(\boldsymbol{x}, t) e^{-\mathrm{i}\boldsymbol{k}\cdot\boldsymbol{x}} d\boldsymbol{x} \equiv \mathcal{F}[A(\boldsymbol{x}, t)], \tag{32}$$

where $\boldsymbol{k}$ are the wave vectors of integers. The time-evolution equations of $u_i(\boldsymbol{k}, t)$, $w_i(\boldsymbol{k}, t)$, $\theta(\boldsymbol{k}, t)$ in the wave vector space are

$$(\partial_t + 2\nu k^2) u_i(\boldsymbol{k}, t) = - P_{ij}(\boldsymbol{k}) \mathcal{F}[(\boldsymbol{u}\cdot\nabla)\boldsymbol{u}]_j = N_i^u(\boldsymbol{k}, t), \tag{33}$$

$$(\partial_t + 2\alpha k^2) w_i(\boldsymbol{k}, t) = - P_{ij}(\boldsymbol{k}) \mathcal{F}[(\boldsymbol{u}\cdot\nabla)\boldsymbol{w}]_j = N_i^w(\boldsymbol{k}, t), \tag{34}$$

$$(\partial_t + 2\kappa k^2) \theta(\boldsymbol{k}, t) = - \mathcal{F}[(\boldsymbol{u}\cdot\nabla)\theta] = N^\theta(\boldsymbol{k}, t), \tag{35}$$

respectively, where $P_{ij}(\boldsymbol{k}) = \delta_{ij} - k_i k_j / k^2$ is the projection operator. Hereafter, for the sake of simplicity of expression, the box size L_{box} is assumed to be infinitely large, so that the sum over the wave vector is understood to be equal to the integral over the wave vector. Under the assumptions of statistical homogeneity and isotropy, the isotropic spectra of the kinetic energy of the fluid per unit mass, the pseudokinetic energy of the passive vector per unit mass, and the variance of the passive scalar are defined by

$$E_u(t) = \frac{1}{2}\langle \boldsymbol{u}^2(\boldsymbol{x}, t)\rangle = \frac{3}{2} u_0^2 = \int_0^\infty E_u(k, t) dk, \tag{36}$$

$$E_w(t) = \frac{1}{2}\langle \boldsymbol{w}^2(\boldsymbol{x}, t)\rangle = \frac{3}{2} w_0^2 = \int_0^\infty E_w(k, t) dk, \tag{37}$$

$$E_\theta(t) = \frac{1}{2}\langle \theta^2(\boldsymbol{x}, t)\rangle = \frac{1}{2} \theta_0^2 = \int_0^\infty E_\theta(k, t) dk, \tag{38}$$

respectively. Then the evolution equations for the spectra are written

$$(\partial_t + 2\nu_A k^2) E_A(k) = T_A(k), \tag{39}$$

where A represents u, w, and θ, ν_u denotes the kinematic viscosity ν, ν_w represents α, and ν_θ represents κ; and

$$T_u(k) = \int_{|\boldsymbol{k}|=k} \mathcal{R}\langle [\boldsymbol{u}^*(\boldsymbol{k}) \cdot \boldsymbol{N}^u(\boldsymbol{k})]\rangle \, d\Omega(\boldsymbol{k}), \tag{40}$$

$$T_w(k) = \int_{|\boldsymbol{k}|=k} \mathcal{R}\langle [\boldsymbol{w}^*(\boldsymbol{k}) \cdot \boldsymbol{N}^w(\boldsymbol{k})]\rangle \, d\Omega(\boldsymbol{k}), \tag{41}$$

$$T_\theta(k) = \int_{|\boldsymbol{k}|=k} \mathcal{R}\langle [\theta^*(\boldsymbol{k}) N^\theta(\boldsymbol{k})]\rangle \, d\Omega(\boldsymbol{k}), \tag{42}$$

where $\mathcal{R}$ denotes the real part and $d\Omega(\boldsymbol{k})$ is the solid angle. The functions $T_A(k)$ are called the transfer functions, arising from the convective term of the original equation under the assumption of incompressibility. From Eqs. (8) to (10), it follows that

$$\int_0^\infty T_A(k) dk = 0. \tag{43}$$

Then, the transfer fluxes across the wave number k are defined by

$$\Pi_A(k) = \int_k^\infty T_A(k')dk'. \tag{44}$$

The mean rates of dissipation of the kinetic energy, pseudokinetic energy and variance per unit mass are defined by

$$\overline{\epsilon} = \nu\langle(\nabla \boldsymbol{u})^2\rangle = \nu\langle\boldsymbol{\omega}^2\rangle = 2\nu\int_0^\infty k^2 E_u(k)dk, \tag{45}$$

$$\overline{\epsilon}_w = \alpha\langle(\nabla \boldsymbol{w})^2\rangle = \alpha\langle(\nabla\times\boldsymbol{w})^2\rangle = 2\alpha\int_0^\infty k^2 E_w(k)dk, \tag{46}$$

$$\overline{\chi} = \kappa\langle(\nabla\theta)^2\rangle = 2\kappa\int_0^\infty k^2 E_\theta(k)dk. \tag{47}$$

As the pseudokinetic energy of the passive scalar is conserved by the convective term and the 4/3 law for Eq.(29) holds, it is reasonable to expect that the pseudokinetic energy is transferred towards high wave numbers by the turbulent flow through the inertial (convective) range, and dissipated (smeared) by the pseudoviscosity. In this case, the dimensional argument yields the Kolmogorov microscales in space, time and velocity as

$$\tau = (\nu/\bar{\epsilon})^{1/2}, \quad \eta = (\nu^3/\bar{\epsilon})^{1/4}, \quad u_\eta = (\nu\bar{\epsilon})^{1/4}, \tag{48}$$

$$\tau_w = \mathrm{Sc}_\alpha^{-1}\tau_\eta, \quad \eta_w = \mathrm{Sc}_\alpha^{-1}\eta, \quad w_\eta = \bar{\epsilon}_w^{1/2}\tau_w^{1/2}, \tag{49}$$

$$\tau_\theta = \mathrm{Sc}^{-1}\tau_\eta, \quad \eta_\theta = \mathrm{Sc}^{-1}\eta, \quad \theta_\eta = \bar{\chi}^{1/2}\tau_\theta^{1/2}, \tag{50}$$

respectively, where $\mathrm{Sc}_\alpha = \nu/\alpha$ and $\mathrm{Sc} = \nu/\kappa$. In this study, we consider only the case such that $\mathrm{Sc}_\alpha = \mathrm{Sc} = 1$, so that $\eta = \eta_w = \eta_\theta$.

In the inertial-convective range ($k_d \ll k \ll k_L$), where $k_d = 1/\eta$ and k_L is a wave number corresponding to the integral scale, Kolmogorov's arguments yield

$$E_u(k) = C_K\bar{\epsilon}^{2/3}k^{-5/3}, \tag{51}$$

$$E_w(k) = C_K^w\bar{\epsilon}^{-1/3}\bar{\epsilon}_w k^{-5/3}, \tag{52}$$

$$E_\theta(k) = C_{\mathrm{OC}}\bar{\epsilon}^{-1/3}\bar{\chi}k^{-5/3}, \tag{53}$$

where C_K and C_{OC} are the Kolmogorov and Obukhov-Corrsin constants and C_K^w is a nondimensional constant.

B. Equations of vorticity, pseudo vorticity and scalar gradient

The vorticity, pseudovorticity and scalar gradient are defined as

$$\boldsymbol{\omega} = \nabla\times\boldsymbol{u}, \quad \boldsymbol{\zeta} = \nabla\times\boldsymbol{w}, \quad \boldsymbol{g} = \nabla\theta, \tag{54}$$

respectively. Then the evolution equations of $\boldsymbol{\omega}$, $\boldsymbol{\zeta}$, and $\boldsymbol{g}$ can be derived as

$$\frac{\partial}{\partial t}\omega_i + (\boldsymbol{u}\cdot\nabla)\omega_i = (\boldsymbol{\omega}\cdot\nabla)u_i + \nu\nabla^2\omega_i, \tag{55}$$

$$\frac{\partial}{\partial t}\zeta_i + (\boldsymbol{u}\cdot\nabla)\zeta_i = (\boldsymbol{\zeta}\cdot\nabla)u_i + \epsilon_{ijk}(\partial_j w_n)(\partial_k u_n) + \alpha\nabla^2\zeta_i, \tag{56}$$

$$\frac{\partial}{\partial t}g_i + (\boldsymbol{u}\cdot\nabla)g_i = -(\boldsymbol{g}\cdot\nabla)u_i + \kappa\nabla^2 g_i, \tag{57}$$

where ϵ_{ijk} is the alternating unit tensor. The first terms of the right-hand side of the above equations represent the amplification of the gradient fields due to the stretching action of the turbulence. The second term of the right-hand side of Eq. (56) includes the effect of the rotation of the pseudovorticity with respect to the eigenvector of the rate of strain tensor of the turbulence. $\langle \boldsymbol{\omega}^2 \rangle$ is the enstrophy, and we call $\langle \boldsymbol{\zeta}^2 \rangle$ the pseudoenstrophy. We define the normalized skewnesses as [36]

$$S_K^u = \frac{\left\langle \left(\frac{\partial u_1}{\partial x_1} \right)^3 \right\rangle}{\left\langle \left(\frac{\partial u_1}{\partial x_1} \right)^2 \right\rangle^{3/2}}, \tag{58}$$

$$S_K^w = \frac{\left\langle \left(\frac{\partial u_1}{\partial x_1} \right) \left[\left(\frac{\partial w_1}{\partial x_1} \right)^2 + \left(\frac{\partial w_2}{\partial x_1} \right)^2 + \left(\frac{\partial w_3}{\partial x_1} \right)^2 \right] \right\rangle}{\left\langle \left(\frac{\partial u_1}{\partial x_1} \right)^2 \right\rangle^{1/2} \left\langle \left(\frac{\partial w_1}{\partial x_1} \right)^2 + \left(\frac{\partial w_2}{\partial x_1} \right)^2 + \left(\frac{\partial w_3}{\partial x_1} \right)^2 \right\rangle}, \tag{59}$$

$$S_K^\theta = \frac{\left\langle \left(\frac{\partial u_1}{\partial x_1} \right) \left(\frac{\partial \theta}{\partial x_1} \right)^2 \right\rangle}{\left\langle \left(\frac{\partial u_1}{\partial x_1} \right)^2 \right\rangle^{1/2} \left\langle \left(\frac{\partial \theta}{\partial x_1} \right)^2 \right\rangle}. \tag{60}$$

IV. NUMERICAL SIMULATIONS

We carried out DNSs of Eqs. (3), (5), and (7) using the pseudospectral method and fourth-order Runge-Kutta-Gill method [37]. To avoid aliasing errors, we selected a cutoff wave number of $k_c = 2\sqrt{2}/3k_{\max}$. To achieve a statistically steady state, we added an external random forces $\boldsymbol{f}^u(\boldsymbol{x}, t)$, $\boldsymbol{f}^w(\boldsymbol{x}, t)$ and a source $f^\theta(\boldsymbol{x}, t)$, which are mutually independent and act only at large scales to the right-hand side of the relevant equations. These are Gaussian white noise variables with means of zero and variances defined by

$$\left\langle f_i^u(\boldsymbol{k}, t) f_j^u(-\boldsymbol{k}, s) \right\rangle = \frac{1}{2} P_{ij}(\boldsymbol{k}) \frac{F_u(k)}{2\pi k^2} \delta(t - s), \tag{61}$$

$$\left\langle f_i^w(\boldsymbol{k}, t) f_j^w(-\boldsymbol{k}, s) \right\rangle = \frac{1}{2} P_{ij}(\boldsymbol{k}) \frac{F_w(k)}{2\pi k^2} \delta(t - s), \tag{62}$$

$$\langle f^\theta(\boldsymbol{k}, t) f^\theta(-\boldsymbol{k}, s) \rangle = \frac{F_\theta(k)}{2\pi k^2} \delta(t - s), \tag{63}$$

respectively. The spectra are set to

$$F_A(k) = \begin{cases} \frac{\varepsilon_{\text{in}}^A}{k_{\text{high}} - k_{\text{low}}} & \text{for } k_{\text{low}} \leqslant k \leqslant k_{\text{high}}, \\ 0 & \text{otherwise.} \end{cases} \tag{64}$$

The injection rate for $\varepsilon_{\text{in}}^\theta$ is selected to be equal to one component of $\boldsymbol{u}$ and $\boldsymbol{w}$, as follows:

$$\varepsilon_{\text{in}}^{u,w} = \int_0^\infty F_{u,w}(k)\, dk, \tag{65}$$

$$\varepsilon_{\text{in}}^\theta = \int_0^\infty F_\theta(k)\, dk = \frac{1}{3} \varepsilon_{\text{in}}^{u,w}. \tag{66}$$

TABLE I. DNS parameters and time-averaged turbulent statistics.

	Run A	Run B	Run C
$2k_{\max}$	512	512	1024
$[k_{\rm low}, k_{\rm high}]$	[2, 3]	[2, 3]	[2, 3]
$\varepsilon_{\rm in}^{u}$	0.45	2.7	0.3
$\varepsilon_{\rm in}^{w}$	0.45	2.7	0.3
$\varepsilon_{\rm in}^{\theta}$	0.15	0.9	0.1
ΔT	5×10^{-4}	2×10^{-4}	10^{-4}
ν	0.001	0.001	2×10^{-4}
$N_T \Delta T / T^E$	24.3	6.53	2.75
R_λ	144.8	196.2	315.0
$k_{\max}\eta$	1.72	1.12	1.16
$\bar{E}_u$	1.19	3.89	0.99
$\bar{E}_w$	0.75	2.74	0.62
$\bar{E}_\theta$	0.19	0.72	0.16
$\bar{\epsilon}$	0.46	2.64	0.33
$\bar{\epsilon}_w$	0.44	2.85	0.31
$\bar{\chi}$	0.14	1.00	0.10
$L_u^{\rm int}$	0.73	0.74	0.72
$L_w^{\rm int}$	0.75	0.75	0.75
$L_\theta^{\rm int}$	0.50	0.48	0.51
λ_u	0.16	0.12	7.7×10^{-2}
λ_w	0.13	9.8×10^{-2}	6.3×10^{-2}
λ_θ	0.09	6.6×10^{-2}	4.3×10^{-2}
T_E	0.82	0.45	0.86
S_K^u	−0.54	−0.51	−0.54
S_K^w	−0.47	−0.40	−0.42
S_K^θ	−0.50	−0.44	−0.45

The Taylor microscale, the integral scale, and the Taylor microscale Reynolds number R_λ are defined as

$$\lambda_u^2 = \frac{\langle u_1^2 \rangle}{\langle (\partial u_1/\partial x_1)^2 \rangle} = 15 u_0^2 \Big(\frac{\nu}{\bar{\epsilon}} \Big), \tag{67}$$

$$L_u^{\rm int} = \frac{3\pi}{4} \frac{\int_0^\infty k^{-1} E_u(k)\, dk}{\int_0^\infty E_u(k) dk}, \tag{68}$$

$$R_\lambda = u_0 \lambda / \nu, \tag{69}$$

respectively, and the corresponding micro- and integral scales are defined similarly.

The large eddy turnover time is defined as $T_E = L_u^{\rm int}/u_0$.

The simulation code was parallelized with MPI and OPENMP, and the computations were mostly carried out on the Plasma Simulator at the National Institute of Fusion Science (NIFS), Toki, Japan. Three runs were carried out. The largest number of grid points is 1024^3, and various statistical values from the runs are summarized in Table I. As the results for Runs A and B are qualitatively similar to those of Run C, we focus on the results of Run C in the following discussion.

V. RESULTS

A. Time histories of simulations

The time variation of the dissipation rates and the skewness for Run C after the transient time are shown in Figs. 1 and 2. They vary slowly over time, which confirms that the statistical steady

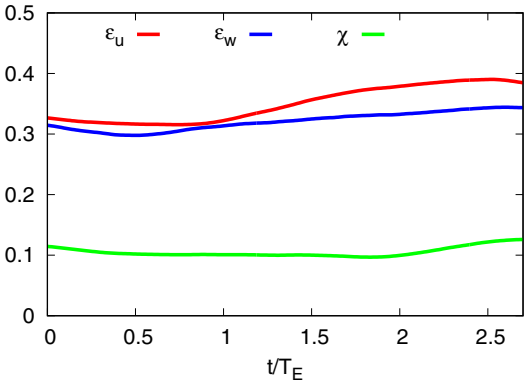

FIG. 1. Time evolution of dissipation rates of the kinetic energy, pseudokinetic energy, and scalar variance.

state was achieved. In the steady state, the external input rates of the (pseudo)kinetic energy and scalar variance balance the dissipations, $\bar{\epsilon}^A = \epsilon^A_{\rm in}$. It then follows from the statistical isotropy and Eqs. (45), (46), and (47) that, in the context of the present problem with $\mathrm{Sc}_\alpha = 1$,

$$\frac{\bar{\epsilon}}{\nu} = \langle \boldsymbol{\omega}^2 \rangle = \langle \boldsymbol{\zeta}^2 \rangle = 3\langle \boldsymbol{g}^2 \rangle = \varepsilon^A_{\rm in}, \tag{70}$$

which is approximately satisfied by the computation. All of the statistical quantities were calculated as time averages over the period of the simulation for approximately three large eddy turnover times.

B. Energy spectra and fluxes

Using the Kolmogorov variables, we normalize the spectra as

$$E^*_u(k\eta) = \bar{\epsilon}^{-1/4}\nu^{-5/4}E_u(k), \tag{71}$$

$$E^*_w(k\eta) = \bar{\epsilon}_w^{-1}\bar{\epsilon}^{3/4}\alpha^{-2}\nu^{3/4}E_w(k), \tag{72}$$

$$E^*_\theta(k\eta) = \chi^{-1}\bar{\epsilon}^{3/4}\kappa^{-2}\nu^{3/4}E_\theta(k). \tag{73}$$

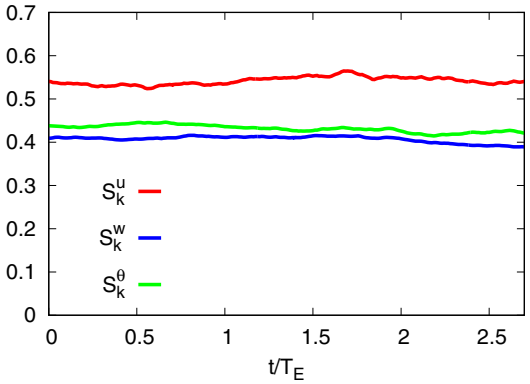

FIG. 2. Time evolution of the skewnesses of the spatial derivatives.

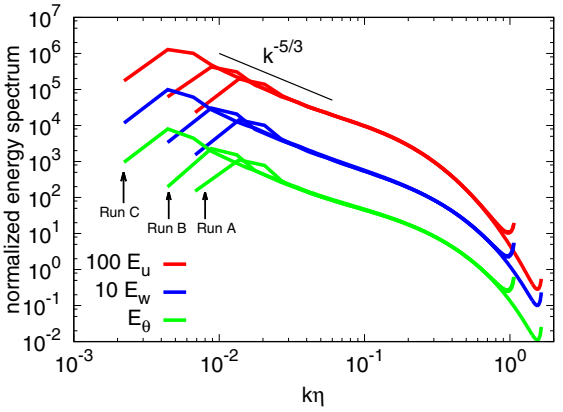

FIG. 3. Normalized energy spectra over three runs. The straight line indicates a gradient of $-5/3$. For ease of visibility, the curves of $E_u^*(k)$ and $E_w^*(k)$ are shifted by 100 and 10, respectively.

The normalized spectra are plotted in Fig. 3. For ease of visibility, the curves of $E_u^*(k)$ and $E_w^*(k)$ are shifted by 100 and 10, respectively. All curves, including $E_w^*(k)$, collapse excellently onto a single curve for $k\eta \in [0.01, 1]$, which indicates that an approximate $-5/3$ power law holds, as expected based on Kolmogorov-Obukhov-Corrsin theory. For $k\eta > 0.3$, E_w^* and E_θ^* decay slower than E_u^*, meaning that E_w and E_θ are excited more strongly than E_u at large wave numbers in the dissipative range.

To compute the constants C_K, C_K^w, and C_{OC}, the compensated spectra for Run C,

$$\Psi_u(k\eta) = \bar{\epsilon}^{-2/3} k^{5/3} E_u(k), \tag{74}$$

$$\Psi_w(k\eta) = \bar{\epsilon}_w^{-1} \bar{\epsilon}^{1/3} k^{5/3} E_w(k), \tag{75}$$

$$\Psi_\theta(k\eta) = \bar{\chi}^{-1} \bar{\epsilon}^{1/3} k^{5/3} E_\theta(k), \tag{76}$$

are plotted in Fig. 4. We obtained the mean values at wave numbers $k\eta \in [0.025, 0.035]$ in the valley [38] as

$$C_K = 1.57, \quad C_K^w = 0.99, \quad C_{\mathrm{OC}} = 0.67. \tag{77}$$

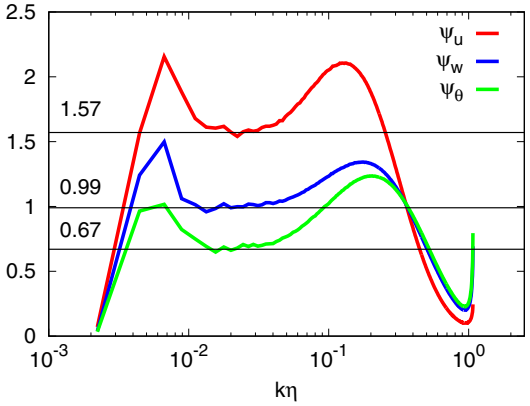

FIG. 4. Compensated energy spectra for Run C.

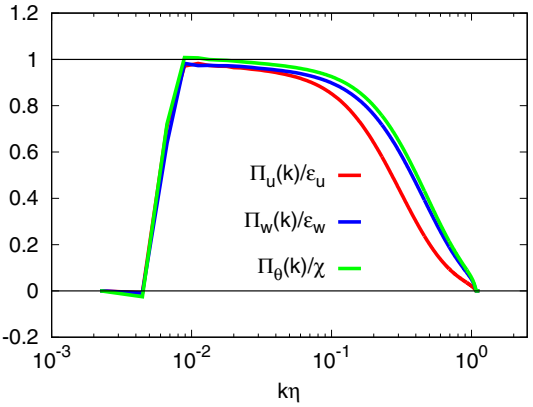

FIG. 5. Normalized energy flux spectra for Run C. The red line is for $\Pi_u/\bar{\epsilon}$, blue is for $\Pi_w/\bar{\epsilon}_w$, and green is for $\Pi_\theta/\bar{\chi}$.

The Kolmogorov and Obukhov-Corrsin constants, $C_K = 1.57$ and $C_{\rm OC} = 0.67$, respectively, are consistent with those quoted in the literature [2,11,25,37–39]. In agreement with previous studies, we observed that the spectral bump of the passive scalar was strongest and attains higher wave numbers than the kinetic energy. The compensated spectrum of $E_w(k)$ shows a similar trend, but is between those of the kinetic energy and the passive scalar. We examine the spectral bump in more detail below.

The normalized spectra of the energy transfer fluxes are plotted in Fig. 5. All of the curves are close to unity for $0.005 < k\eta < 0.03$, but the curve of Π_θ decays more slowly than Π_u, followed by Π_w in the far dissipation range. These results are consistent with strong excitations of E_w and E_θ at high wave numbers.

C. Structure functions: 4/5 Law and 4/3 Laws

The normalized structure functions $S_u^*(r)$, $S_w^*(r)$, and $S_\theta^*(r)$ are defined as

$$S_u^*(r) = -\frac{\langle(\delta u_L)^3\rangle}{\frac{4}{5}\bar{\epsilon}r}, \tag{78}$$

$$S_w^*(r) = -\frac{\langle(\delta u_L)|\delta \boldsymbol{w}|^2\rangle}{\frac{4}{3}\bar{\epsilon}_w r}, \tag{79}$$

$$S_\theta^*(r) = -\frac{\langle(\delta u_L)(\delta\theta)^2\rangle}{\frac{4}{3}\bar{\chi}r}, \tag{80}$$

and shown in Fig. 6. The plateaus of the three curves approach unity from below in the range $r \sim 100\eta$, indicating that the Kolmogorov 4/5 and 4/3 laws hold for S_u^* and S_w^*, and the Yaglom 4/3 law holds for S_θ^*. The fact that all of the S_A^* curves are smaller than unity is consistent with previous studies [1,2]. Careful examination reveals that the plateau of S_θ^* appears roughly in the range of $20 < r\eta < 80$ and that of S_u^* occurs at larger scales, $60 < r\eta < 200$, while the plateau of S_w^* is $40 < r\eta < 200$, which is wider than that of the two curves. Moreover, the S_w^* curve collapses to S_θ^* in the dissipation range $r/\eta < 10$. These trends are consistent with the high excitations of $E_w(k)$ and $E_\theta(k)$ shown in Fig. 4, and the collapse of $\Pi_w(k)$ and $\Pi_\theta(k)$ at high wave numbers in Fig. 5.

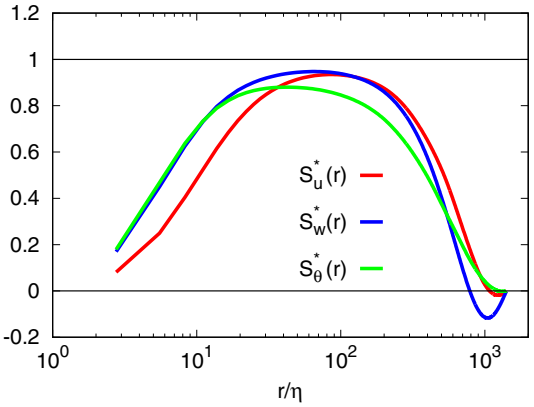

FIG. 6. Normalized third-order structure functions of Run C.

D. Spectra of pressure and pseudopressure

The spectra of the pressure and pseudopressure are defined as

$$\langle p^2 \rangle = \int_0^\infty E_p(k)dk, \quad \langle q^2 \rangle = \int_0^\infty E_q(k)dk, \tag{81}$$

and normalized in terms of the Kolmogorov microscales as

$$E_p^*(k\eta) = u_\eta^{-4}\eta^{-1}E_p(k), \quad E_q^*(k\eta) = (u_\eta w_\eta)^{-2}\eta_w^{-1}E_q(k), \tag{82}$$

respectively. These are shown in Fig. 7 for Run C. We observed that the spectrum $E_q(k)$ is smaller than that of $E_p(k)$ at all wave numbers, but the overall functional forms are very similar. We examined the two spectra in further detail by normalizing them as $E_p(k\eta)/E_p(k_*\eta)$ (red) and $E_q(k\eta)/E_q(k_*\eta)$ (blue), where $k_*\eta = 0.03$ is selected such that the nearly straight portions collapse well. The resulting curves are plotted in Fig. 8. We can clearly see that the two shifted spectra collapsed excellently for $k\eta > 0.02$.

To investigate these spectra in more detail, we plotted the ratio $E_p(k)/E_q(k)$ in the inset of Fig. 8. The ratio increases quickly, from 2 to 4, as the wave number increases, then remains at approximately 4.5 in the power law range, which means that both spectra $E_p(k)$ and $E_q(k)$ obey the same power law as $k^{-\beta}$ with an exponent of $\beta \approx 2$, which is slightly shallower than the

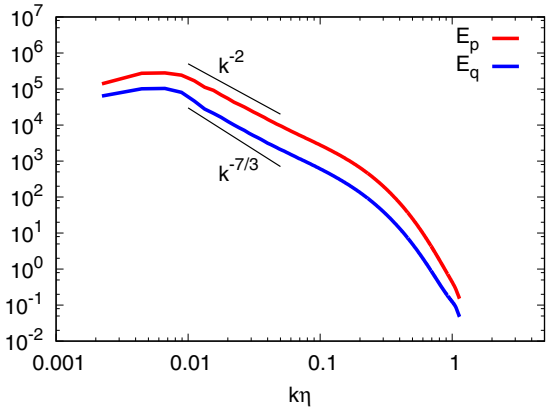

FIG. 7. Spectra of pressure and pseudopressure for Run C.

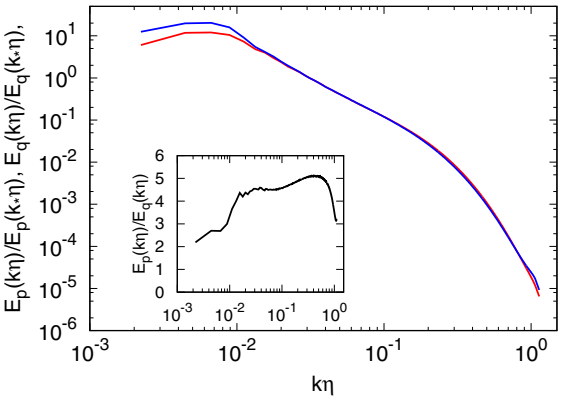

FIG. 8. Comparison of shifted spectra $E_p(k\eta)/E_p(k_*\eta)$ (red) and $E_q(k\eta)/E_q(k_*\eta)$ (blue) of the pressure and pseudopressure for Run C, respectively. $k_*\eta = 30$ is chosen such that the portions that are almost straight collapse well. The inset shows the ratio $E_p(k\eta)/E_q(k\eta)$ for Run C.

$k^{-7/3}$ Kolmogorov scaling. This is due to the relatively lower Reynolds numbers, which have been studied recently using DNSs [40,41]. In the case of wave numbers in the dissipation range, the ratio increases then quickly falls off.

The two-point correlation functions of the Laplacians of the pressure and pseudopressure are written as

$$\langle \Delta p(\boldsymbol{x}+\boldsymbol{r})\Delta p(\boldsymbol{x})\rangle = \langle S_{uu}(\boldsymbol{x}+\boldsymbol{r})S_{uu}(\boldsymbol{x})\rangle, \tag{83}$$

$$\langle \Delta q(\boldsymbol{x}+\boldsymbol{r})\Delta q(\boldsymbol{x})\rangle = \langle S_{uw}(\boldsymbol{x}+\boldsymbol{r})S_{uw}(\boldsymbol{x})\rangle, \tag{84}$$

where

$$S_{uu}(\boldsymbol{x}) = -\nabla \boldsymbol{u}(\boldsymbol{x}) : \nabla \boldsymbol{u}(\boldsymbol{x}), \tag{85}$$

$$S_{uw}(\boldsymbol{x}) = -\nabla \boldsymbol{u}(\boldsymbol{x}) : \nabla \boldsymbol{w}(\boldsymbol{x}). \tag{86}$$

The Fourier transform of Eqs. (83) and (84) leads to

$$E_p(k) = k^{-4} 4\pi k^2 \langle |S_{uu}(\boldsymbol{k})|^2\rangle, \tag{87}$$

$$E_q(k) = k^{-4} 4\pi k^2 \langle |S_{uw}(\boldsymbol{k})|^2\rangle, \tag{88}$$

under the assumption of statistical isotropy. As $E_q(k) < E_p(k)$ for all wave numbers, as shown in Fig. 7, we have

$$\langle |S_{uw}(\boldsymbol{k})|^2\rangle < \langle |S_{uu}(\boldsymbol{k})|^2\rangle. \tag{89}$$

Using Parseval's equality, we obtain

$$\langle [S_{uw}(\boldsymbol{x})]^2\rangle = \int \langle |S_{uw}(\boldsymbol{k})|^2\rangle \, d\boldsymbol{k} < \int \langle |S_{uu}(\boldsymbol{k})|^2\rangle \, d\boldsymbol{k} = \langle [S_{uu}(\boldsymbol{x})]^2\rangle. \tag{90}$$

It follows from the Schwartz inequality that the two-point correlation functions satisfy

$$\langle S_{uu}(\boldsymbol{x}+\boldsymbol{r})S_{uu}(\boldsymbol{x})\rangle \leqslant \langle [S_{uu}(\boldsymbol{x})]^2\rangle, \tag{91}$$

$$\langle S_{uw}(\boldsymbol{x}+\boldsymbol{r})S_{uw}(\boldsymbol{x})\rangle \leqslant \langle [S_{uw}(\boldsymbol{x})]^2\rangle. \tag{92}$$

The source terms Eqs. (83) and (84) are written as

$$[S_{uu}]_{ij} = \tfrac{1}{4}(e_{ik} + a_{ik})(e_{kj} + a_{kj}), \tag{93}$$

$$[S_{uw}]_{ij} = \tfrac{1}{4}(e_{ik} + a_{ik})\left(e^w_{kj} + a^w_{kj}\right), \tag{94}$$

where $\boldsymbol{e}$ and $\boldsymbol{a}$ are the symmetric and antisymmetric parts of the gradient tensor. We consider a small domain in which both $\boldsymbol{a}$ and $\boldsymbol{a}^w$ are zero for simplicity. For S_{uu}, the alignment between the eigenvectors of $\boldsymbol{e}$ and $\boldsymbol{e}$ is perfect and unchanged, but in the case of S_{uw} the eigenvectors of $\boldsymbol{e}$ and $\boldsymbol{e}^w$ are imperfectly aligned, and the alignment depends on the position and time due to the misalignment effects included in the second term of the right-hand side of Eq. (56). This means that the geometrical coherency of $\nabla \boldsymbol{u} : \nabla \boldsymbol{w}$ is weaker than that of $\nabla \boldsymbol{u} : \nabla \boldsymbol{u}$. Furthermore, as we will see in the next subsection, the pseudovorticity production is weaker than the vorticity production. Hence, we expect the amplitudes of $\nabla \boldsymbol{w}$ to be smaller than those of $\nabla \boldsymbol{u}$. Therefore it is physically reasonable to observe that $\langle [S_{uw}(\boldsymbol{x})]^2 \rangle < \langle [S_{uu}(\boldsymbol{x})]^2 \rangle$.

E. Spectra of production of gradients of velocity, passive vector, and scalar

The vorticity is enhanced by the stretching action due to the straining motion, as shown by Eq. (55). However, the pseudovorticity is excited by the stretching action and the second term of the right-hand side of Eq. (56). It is interesting to observe the wave number ranges that contribute to the production of vorticity, pseudovorticity, and the scalar gradient. For this purpose, we investigated the spectra

$$\sigma^*_\omega(k) = \frac{1}{\langle \boldsymbol{\omega}^2 \rangle^{3/2} \eta} \int_{|\boldsymbol{k}|=k} \langle \boldsymbol{\omega}(-\boldsymbol{k}) \cdot \mathcal{F}[S : \boldsymbol{\omega}] \rangle \, d\Omega(\boldsymbol{k}), \tag{95}$$

$$\sigma^*_\zeta(k) = \sigma^*_{\zeta,\mathrm{str}}(k) + \sigma^*_{\zeta,\mathrm{crs}}(k), \tag{96}$$

$$\sigma^*_{\zeta,\mathrm{str}}(k) = \frac{1}{\langle \boldsymbol{\zeta}^2 \rangle \langle \boldsymbol{\omega}^2 \rangle^{1/2} \eta} \int_{|\boldsymbol{k}|=k} \langle \boldsymbol{\zeta}(-\boldsymbol{k}) \cdot \mathcal{F}[S : \boldsymbol{\zeta}] \rangle \, d\Omega(\boldsymbol{k}), \tag{97}$$

$$\sigma^*_{\zeta,\mathrm{crs}}(k) = \frac{1}{\langle \boldsymbol{\zeta}^2 \rangle \langle \boldsymbol{\omega}^2 \rangle^{1/2} \eta} \int_{|\boldsymbol{k}|=k} \langle \boldsymbol{\zeta}(-\boldsymbol{k}) \cdot \mathcal{F}[(\nabla \boldsymbol{u})^T \times (\nabla \boldsymbol{w})^T] \rangle \, d\Omega(\boldsymbol{k}), \tag{98}$$

$$\sigma^*_g(k) = -\frac{1}{\langle \boldsymbol{g}^2 \rangle \langle \boldsymbol{\omega}^2 \rangle^{1/2} \eta} \int_{|\boldsymbol{k}|=k} \langle \boldsymbol{g}(-\boldsymbol{k}) \cdot \mathcal{F}[S : \boldsymbol{g}] \rangle \, d\Omega(\boldsymbol{k}), \tag{99}$$

and plotted them in Fig. 9. Note that, as the variances in front of the integrals satisfy Eq. (70), the curves of σ^*_ω and σ^*_ζ can be directly compared in terms of actual amplitudes. If we multiplied the curve of σ^*_g by $1/3$, we could compare it with the other two curves. The terms $\sigma_{\zeta,\mathrm{str}}$ and $\sigma_{\zeta,\mathrm{crs}}$ are contributions arising from the first and second terms of the right-hand side of Eq. (56), respectively. $\sigma_{\zeta,\mathrm{str}}$ is positive, meaning that the production of pseudovorticity is due to the stretching effects of the turbulence, while $\sigma_{\zeta,\mathrm{crs}}$ is negative and diminishes the production by destroying the geometrical coherency between $\nabla \boldsymbol{u}$ and $\nabla \boldsymbol{w}$. Therefore, the total production of the pseudovorticity is positive, but less intensive than the vorticity production, which in turn leads to the fact that $\langle [S_{uw}(\boldsymbol{x})]^2 \rangle < \langle [S_{uu}(\boldsymbol{x})]^2 \rangle$ as seen in Eq. (90). As indicated in Eq. (70), it is the case that $\nu \langle \boldsymbol{\omega}^2 \rangle = \bar{\epsilon} = \bar{\epsilon}_w = \alpha \langle \boldsymbol{\zeta}^2 \rangle$ and $\sigma_{\zeta,\mathrm{str}} < \sigma_{\omega,\mathrm{str}}$. At first glance, these two facts appear contradictory. The resolution of this contradiction can be obtained from the spectra. As $E_w(k)$ decays more slowly than $E_u(k)$ in the dissipation range, the longer tail of $E_w(k)$ leads to the same dissipation rate as $\bar{\epsilon}$, due to Eqs. (45) and (46).

σ^*_ω, σ^*_ζ, and σ^*_g are positive at all wave numbers and have peaks at $k\eta \sim 0.2$. When the wave number decreases, σ^*_ω and σ^*_ζ decrease but, surprisingly, σ^*_g remains finite even at very low wave numbers, $k\eta < 0.1$. Although we cannot explain why σ^*_g is finite, we note that the ramp-cliff or

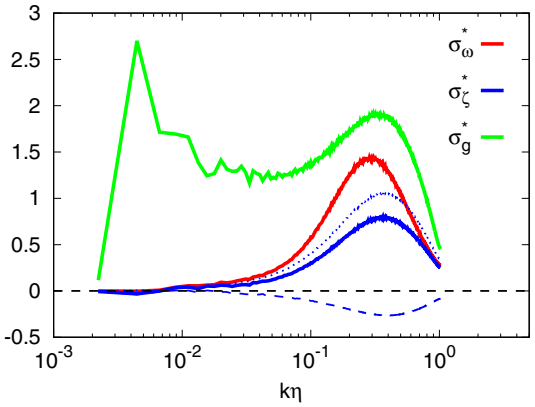

FIG. 9. Spectra of production terms of enstrophy, pseudoenstrophy and scalar gradient variance. Red: σ_ω^*; blue: σ_ζ^*; green: σ_g^*. The blue dotted line denotes $\sigma_{\zeta,\mathrm{str}}^*$ and the blue broken line represents $\sigma_{\zeta,\mathrm{crs}}^*$.

mesa-canyon structure of the scalar field characterized by a large scalar gradient in the DNSs and experiments has very long-range coherency, of integral length order or larger [11,15,22,42–46].

F. Bottleneck effects and band-to-band energy transfer

One way to compare the amplitudes of the spectral bumps of $E_u(k)$, $E_w(k)$, and $E_\theta(k)$ on an equal footing is to divide the compensated spectra by their plateau values, the Kolmogorov constant C_K, and the Obukhov-Corrsin constants C_K^w and C_{OC}, respectively. The resulting curves are plotted in Fig. 10. The peak values indicate the bump amplitude with respect to the plateau level. The wave numbers and values of the bump maximum of the curve are denoted k_p^u, k_p^w, k_p^θ and A_p^u, A_p^w, A_p^θ. We then obtain

$$k_p^u = 0.12, \quad k_p^w = 0.18, \quad k_p^\theta = 0.21, \tag{100}$$

$$A_p^u \sim A_p^w = 1.2, \quad A_p^\theta = 1.9. \tag{101}$$

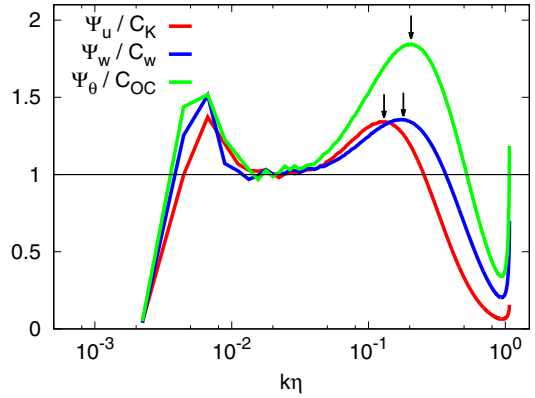

FIG. 10. Measurement of the bottleneck effect. The + symbols denote the peaks of the compensated energy spectrum.

It can readily be seen that the spectral bump of the passive scalar is the largest, and its velocity is lowest, while the passive vector lies between. Thus, the bottleneck effect is strongest for the passive scalar, weakest for the velocity, and intermediate for the passive vector.

Donzis and Sreenivasan [38] showed that the spectral bump decreases with increasing Reynolds number, and suggested nonlocalness in the spectral transfer as a possible mechanism for generating the spectral bump. The spectral bump has been explained as a manifestation of the bottleneck effect [47]. When one or two components in the triad interaction are only weakly excited due to dissipation, the spectral transfer becomes less efficient, so the spectrum piles up at wave numbers just below the dissipation range. If the spectral transfer is dominated by nonlocal interactions, the lack of excitation of one or two components at distant wave numbers would result in a larger pileup of spectral excitation before the beginning of the spectrum rolloff that occurs in the dissipation range. In other words, the stronger the nonlocalness, the larger the spectral bump.

To determine whether this is the case, we analyzed the nonlocalness of the spectral transfer of the scalar variance by comparing it to that of the kinetic and pseudokinetic energy. First, we consider the spectral transfer fluxes of the kinetic energy and the scalar variance, which are written

$$\frac{\Pi(k)}{\overline{\epsilon}} = \int_1^\infty W(\xi, k)\frac{d\xi}{\xi}, \tag{102}$$

$$\frac{\Pi_\theta(k)}{\overline{\chi}} = \int_1^\infty W_\theta(\xi, k)\frac{d\xi}{\xi}, \tag{103}$$

$$\xi = \frac{\max(k, p, q)}{\min(k, p, q)}, \tag{104}$$

where (k, p, q) are the three wave numbers of the triad interaction in the nonlinear and convective terms. ξ is a nonlocalness metric in the triad interaction, with larger ξ indicating more nonlocal interaction, and the functions $W(\xi, k)$ and $W_\theta(\xi, k)$ represent the fractional contributions to the total mean transfer flux from the interactions in the range $[\xi, \xi + d\xi]$. Using the Lagrangian renormalized approximation (LRA) [48–50], Gotoh and Watanabe [51] showed that, in the inertial range at very high Reynolds numbers, the functions $W(\xi)$ and $W_\theta(\xi)$ are asymptotically

$$W(\xi) \sim C_K^2 I_v \left(\frac{4}{9}\xi^{-4/3}\ln\xi + \frac{16}{45}\xi^{-4/3}\right), \tag{105}$$

$$W_\xi(\xi) \sim C_K C_{OC} I_\theta \left(\frac{22}{45}\xi^{-2/3} + \frac{4}{3}\xi^{-4/3}\ln\xi\right), \tag{106}$$

$$I_v = 0.7896, \quad I_\theta = 1.202, \tag{107}$$

respectively. The function $W_\theta(\xi)$ decays more slowly than $W(\xi)$ for large ξ. This means that the spectral transfer of the passive scalar variance is less local than that of the kinetic energy, which is consistent with the bump in the scalar spectrum being larger at higher wave numbers than in the case of the kinetic energy.

The above results are for an infinite Reynolds number and depend on the assumptions of the LRA. To investigate the energy transfer from band to band at finite Reynolds numbers, we introduce a sharp filter G and filtered quantities A_K, which we define as follows:

$$G_K(\boldsymbol{k}) = \begin{cases} 1 & \text{if } K - 0.5 \leqslant |\boldsymbol{k}| < K + 0.5, \\ 0 & \text{otherwise,} \end{cases} \tag{108}$$

$$A_K(\boldsymbol{x}, t) = \mathcal{F}^{-1}[A(\boldsymbol{k}, t)G_K(\boldsymbol{k})]. \tag{109}$$

Then, the spectral transfer functions between bands K and Q are defined in the same way as in Ref. [52]:

$$\mathcal{T}^{u}_{K,Q} = -\frac{1}{\bar{\epsilon}V}\int \boldsymbol{u}_K \cdot [(\boldsymbol{u}\cdot\nabla)\boldsymbol{u}_Q]\, d\boldsymbol{x}, \tag{110}$$

$$\mathcal{T}^{w}_{K,Q} = -\frac{1}{\bar{\epsilon}_w V}\int \boldsymbol{w}_K \cdot [(\boldsymbol{u}\cdot\nabla)\boldsymbol{w}_Q]\, d\boldsymbol{x}, \tag{111}$$

$$\mathcal{T}^{\theta}_{K,Q} = -\frac{1}{\bar{\chi}V}\int \theta_K [(\boldsymbol{u}\cdot\nabla)\theta_Q]\, d\boldsymbol{x}. \tag{112}$$

The numerical results are shown in Fig. 11. A common feature is that they are negative for $K/Q < 1$ and positive for $K/Q > 1$; furthermore, the local minimum and maximum appear in the narrow wave number band, close to $K/Q = 1$, which means that the mean spectral transfer is predominantly local for all $\mathcal{T}^{u}_{K,Q}$, $\mathcal{T}^{w}_{K,Q}$, and $\mathcal{T}^{\theta}_{K,Q}$.

We now examine the effects of the band position Q on the transfer to the band K. For $\mathcal{T}^{u}_{K,Q}$ (top panel of Fig. 11), the curve for $Q\eta \sim 0.005$ (red) has positive peaks at approximately $K/Q = 2$ and reaches distant wave numbers at $Q/K > 10$, while the curve for $Q\eta \sim 0.02$ (blue) is largely negative at $K/Q \sim 1/2$, and exhibits positive peaks at wave numbers near $K/Q = 1$. The curve for $Q\eta \sim 0.15$ (green) has sharp negative and positive peaks at wave numbers close to $K/Q = 1$ but their amplitudes are smaller due to the smaller excitations. The above observations can also be applied to the mean spectral transfer fluxes $\mathcal{T}^{w}_{K,Q}$ and $\mathcal{T}^{\theta}_{K,Q}$.

We now compare the relative strengths of the nonlocalness of the mean spectral transfers for three bands, $Q\eta = 0.005, 0.02, 0.15$, by plotting their absolute values on logarithmic scales in Figs. 12. The solid lines represent positive values and the lines plotted with symbols indicate negative values. The general trend is that the curve of the passive vector is close to that of the velocity for wave numbers between the peak and the band, prior to the rapid decay of the velocity curve, while the passive vector curve is close to that of the passive scalar at high wave number bands. In the case such that $Q\eta = 0.005$, the passive scalar curve (green) decays most slowly, approximately as K^{-2}. On the other hand, the kinetic energy (red) and pseudokinetic energy (blue) curves are very similar for some wave number ratios and decay faster than the passive scalar curve. This means that the spectral transfer of the passive scalar is strongest and the passive vector is slightly less local than the velocity. This observation is consistent with the order of the bump amplitudes of the compensated spectra shown in Fig. 10. However, the above analysis provides a somewhat indirect method for exploring the relationship between the bump strength and nonlocalness of the spectral transfer. A more direct approach is necessary, such as DNSs with restricted nonlocal interactions. This will be the subject of a future study.

Figure 12 shows an interesting and unexpected result: the curves for the kinetic energy change sign at the high end of K/Q, indicating an inverse transfer of kinetic energy. The wave numbers at which the change of sign occurs correspond to approximately $k\eta \approx 0.4$ in the cases of $Q\eta = 0.005, 0.02, 0.15$, where the kinetic energy spectra begin to roll off in the dissipation range, as shown in Fig. 3. This fact can be regarded as one reason for the kinetic energy spectrum decaying faster than the other spectra in the dissipation range. Although the amplitude of the spectral transfer is very low, the trend is clear. Unfortunately, we cannot explain this negative transfer.

VI. DISCUSSION

The key findings of this study are the following. (1) The three spectra have inertial and inertial convective ranges and approximately follow a $k^{-5/3}$ power law, with constants $C^{u}_{K} = 1.57$ for the kinetic energy, $C^{w}_{K} = 0.99$ for the pseudo kinetic energy, and $C_{\mathrm{OC}} = 0.67$ for the passive scalar variance. Their order, $C^{u}_{K} > C^{w}_{K} > C_{\mathrm{OC}}$, reflects the fact that in the inertial-convective range, more efficient spectral transfer is associated with lower constants. (2) The passive scalar has the largest bump, the velocity has the smallest, and that of the passive vector is in between. (3) The spectra

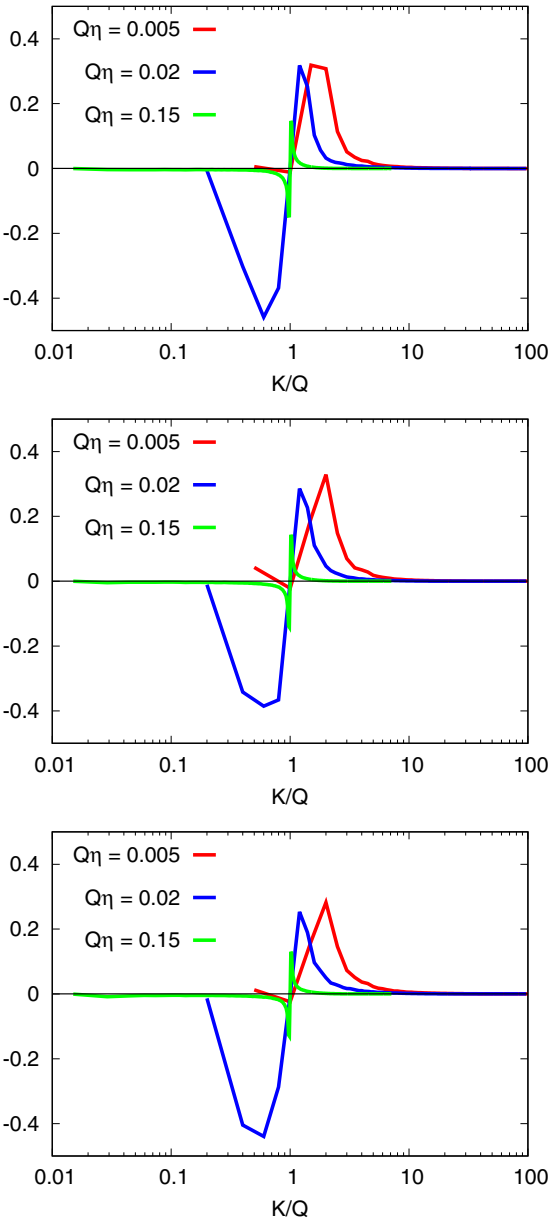

FIG. 11. Band-to-band transfer for Run C. Top: kinetic energy; middle: pseudokinetic energy; bottom: passive scalar variance. Red: $Q\eta = 0.005$; blue: $Q\eta = 0.02$; black: $Q\eta = 0.15$.

and transfer flux spectra of the variances of the passive vector and passive scalar decay slower than those of the kinetic energy in the dissipation range. (4) The cubic moment $\langle(\delta u_L)|\delta \boldsymbol{w}|^2\rangle$ was shown theoretically to obey a $4/3$ power law, similar to Yaglom's $4/3$ law for the passive scalar, and the curve computed by the DNS approaches the $4/3$ law, which is close to the velocity curve at large scales and to the passive scalar curve at small scales.

All of these facts suggest that, for the Reynolds numbers investigated in this study, the behavior of $\boldsymbol{w}$ at large scales is close to $\boldsymbol{u}$ and resembles θ at small scales, and that the transfer efficiency of the passive vector is "intermediate" between the velocity and passive vector.

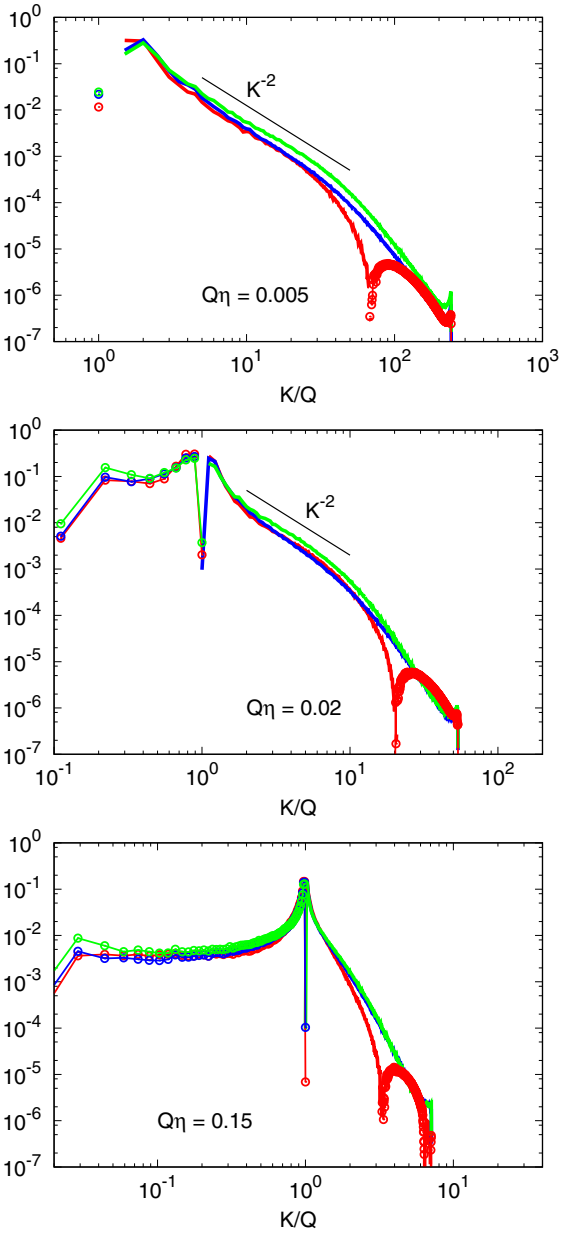

FIG. 12. Comparison between absolute values of the band-to-band spectral transfer on a logarithmic scale for Run C. Lines with circles denote absolute values of negative numbers. The straight line indicates K^{-2}. Top: $Q\eta = 0.005$; middle: $Q\eta = 0.02$; bottom: $Q\eta = 0.15$. Red: kinetic energy; blue: pseudokinetic energy; green: passive scalar variance.

To explore the physics behind the intermediate behavior of the passive vector, we investigated the non-localness of the spectral transfer of the three fields and the pressure and pseudo pressure spectra. Although the spectral transfer of the three fields is basically local in wavenumber space, there are some contributions from non-local spectral transfer. The degree of nonlocalness of the spectral transfer of the passive scalar is stronger than that of the velocity and passive vector. We also

found that the spectral transfer fluxes of the passive vector and passive scalar in the case such that $K/Q > 1$ are positive, but the velocity is negative for K in the far-dissipation range. The pressure spectrum is approximately five times larger than the pseudopressure spectrum at all wave numbers, but their functional forms are very similar. They scale approximately as k^{-2} in the range of wave numbers in which inertial effects are dominant.

One possible interpretation of these observations could be that the action of the pseudopressure is dominant at large scales, but weaker at small scales. Hence, the two- point statistics of the passive vector, such as the spectrum, spectral transfer flux, and cubic moments, resemble those of the velocity at large scales while being closer to the passive scalar at small scales. These differences can be traced back to the difference between the source terms of the Poisson equations for the pressure and the pseudopressure, the second-order nonlinearity in the velocity gradient, or the bilinear nature of the gradients of the velocity and passive vector. At large scales, the pseudopressure is given as the integral of the source term over the entire domain, and is weighted by the Poisson kernel so that the detailed structures of the straining field, whether $\nabla \boldsymbol{u} : \nabla \boldsymbol{u}$ or $\nabla \boldsymbol{u} : \nabla \boldsymbol{w}$, are smoothed out by the integration except for the amplitudes. However, at small scales, both the pressure and pseudopressure tend to be dominated by the local structure, and differences emerge between $\nabla \boldsymbol{u} : \nabla \boldsymbol{u}$ and $\nabla \boldsymbol{u} : \nabla \boldsymbol{w}$. It is plausible that the nonlinearity of the velocity gradients can develop space-time coherency with respect to the amplitudes and geometry, and thus maintain long-lived vortex tubes. However, the passive nature of $\boldsymbol{w}$ means that it cannot maintain such a locally coherent structure, so the pseudopressure cannot behave similarly to the pressure.

It is useful to recall the behavior of turbulence in D dimensions [53]. When the spatial dimension, D, increases, the incompressibility constraint weakens because the number of terms such that $\partial u_i/\partial x_i = 0$ increases with D, thus diminishing the contributions of the pressure. In this case, the relative importance of the convective action increases, meaning that the nonlinearity dominates the small-scale dynamics. One implication of this argument is that the incompressibility condition for the passive vector, which is assured by the pseudopressure, is of secondary importance to the small-scale dynamics of the passive vector, and the convective term is a main player. Therefore, whether the convective term is linear or nonlinear makes a difference at small scales, while the pseudopressure becomes appreciable for large-scale statistics. Indeed, the visualization shows that the structure of the pseudovorticity $\boldsymbol{\zeta}$ resembles that of the passive scalar, being sheet-like rather than tube-like. This will be discussed in a future publication [35].

VII. SUMMARY

In order to explore the physics behind the differences and similarities in the statistical properties between the velocity vector and passive scalar, we have investigated the low order statistics of the passive vector by comparing them with those of the velocity and passive scalar. The passive vector shares dynamics with passive scalar due to convection by turbulent velocity and diffusion, but the incompressibility constraint under the action of pseudopressure is similar to that of turbulent velocity. We analyzed the energy spectrum, pressure spectrum, energy flux, and cubic order structure functions of $\boldsymbol{u}$, $\boldsymbol{w}$, and θ, and compared the gradients of the three fields. Based on this comparison, we conclude that, at the Reynolds numbers investigated in this study, the behavior of $\boldsymbol{w}$ is (1) close to $\boldsymbol{u}$ at large scales due to the nonlocal effects of the pseudopressure and (2) close to θ at small scales. Therefore, the differences between $\boldsymbol{w}$ and θ at large scales are due to the pseudopressure, and their resemblance at small scales is due to the linearity of the convective term. When this interpretation is applied to the velocity, the difference between the velocity and passive scalar at small scales can ultimately be attributed to whether or not the convective term is nonlinear. In other words, the differences arise from the nonlinear dynamics; the kinematic constraints are of secondary importance. It is interesting and important to see whether the above interpretation can also be applied to the high order statistics. Intermittency, high order statistics, and field structure of the passive vector will be reported in a separate paper [35].

ACKNOWLEDGMENTS

The authors thank Dr. Izumi Saito, Dr. Jianchun Wang, and Dr. Tatsuya Yasuda for their helpful discussions and comments. The National Institute for Fusion Science of Japan (NIFS16KNSS076, NIFS18KNSS105) is gratefully acknowledged for providing computational resources. Also Networking, Large-scale Data Analyzing and Information Systems (JHPCN) (jh180009, jh190018) and High Performance Computing (HPC2018) at Nagoya University, and ES at JAMSTEC are acknowledged. The work of T.G. was supported by MEXT KAKENHI (JP) through Grant No. 15H02218, and JSPS KAKENHI Grants No. 17K05734 for H.M. and No. 18K03925 for T.W. are highly appreciated.

[1] T. Gotoh and P. K. Yeung, Passive scalar transport in turbulence, A Computational Perspective, in *Ten Chapters in Turbulence*, edited by P. Davidson, Y. Kaneda, and K. R. Sreenivasan (Cambridge University Press, Cambridge, 2013).

[2] T. Ishihara, T. Gotoh, and Y. Kaneda, Study of high-Reynolds number isotropic turbulence by direct numerical simulation, Annu. Rev. Fluid Mech. **41**, 165 (2009).

[3] A. N. Kolmogorov, The local structure of turbulence in incompressible fluid for very large Reynolds numbers, Dokl. Akad. Nauk. SSSR **30**, 299 (1941).

[4] A. M. Obukhov, The structure of the temperature field in a turbulent flow, Izv. Akad. Nauk. SSSR, Ser. Geogr. and Geophys. **13**, 58 (1949).

[5] S. Corrsin, On the spectrum of isotropic temperature fluctuations in isotropic turbulence, J. Appl. Phys. **22**, 469 (1951).

[6] A. M. Yaglom, On the local structure of a temperature field in a turbulent flow, Dokl. Akad. Nauk. SSSR **69**, 743 (1949).

[7] G. K. Batchelor, Small-scale variation of convected quantities like temperature in turbulent fluid. Part 1. General discussion and the case of small conductivity, J. Fluid Mech. **5**, 113 (1959).

[8] G. K. Batchelor, I. K. Howells, and A. A. Townsend, Small-scale variations of convected quantities like temperature in turbulent fluid. Part 2. The case of large conductivity, J. Fluid Mech. **5**, 134 (1959).

[9] A. Celani, A. Lanotte, A. Mazzino, and M. Vergassola, Universality and Saturation of Intermittency in Passive Scalar Turbulence, Phys. Rev. Lett. **84**, 2385 (2000).

[10] F. Moisy, H. Willaime, J. S. Andersen, and P. Tabeling, Passive Scalar Intermittency in Low Temperature Helium Flows, Phys. Rev. Lett. **86**, 4827 (2001).

[11] T. Watanabe and T. Gotoh, Statistics of a passive scalar in homogeneous turbulence, New J. Phys. **6**, 40 (2004).

[12] T. Watanabe and T. Gotoh, Intermittency in passive scalar turbulence under the uniform mean scalar gradient, Phys. Fluids **18**, 058105 (2006).

[13] H. Stapountzis, B. L. Sawford, J. C. R. Hunt, and R. E. Britter, Structure of the temperature field downwind of a line source in grid turbulence, J. Fluid Mech. **165**, 401 (1986).

[14] J. Jiménez, A. A. Wray, P. G. Saffman, and R. S. Rogallo, The structure of intense vorticity in isotropic turbulence, J. Fluid Mech. **255**, 65 (1993).

[15] T. Gotoh and T. Watanabe, Scalar flux in a uniform mean scalar gradient in homogeneous isotropic steady turbulence, Physica D (Amsterdam) **241**, 141 (2012).

[16] R. H. Kraichnan, Small scale structure of a scalar field convected by turbulence, Phys. Fluids **11**, 945 (1968).

[17] R. H. Kraichnan, Anomalous Scaling of a Randomly Advected Passive Scalar, Phys. Rev. Lett. **72**, 1016 (1994).

[18] L. Ts. Adzhemyan, N. V. Antonov, A. Mazzino, P. Muratore-Ginanneschi, and A. V. Runov, Pressure and intermittency in passive vector turbulence, Europhys. Lett. **55**, 801 (2001).

[19] K. Gawędzki and A. Kupiainen, Anomalous Scaling of the Passive Scalar, Phys. Rev. Lett. **75**, 3834 (1995).
[20] G. Falkovich, K. Gawędzki, and M. Vergassola, Particles and fields in fluid turbulence, Rev. Mod. Phys. **73**, 913 (2001).
[21] A. Celani, M. Cencini, A. Mazzino, and M. Vergassola, Active and passive fields face to face, New J. Phys. **6**, 72 (2004).
[22] A. Celani, A. Lanotte, A. Mazzino, and M. Vergassola, Fronts in passive scalar turbulence, Phys. Fluids **13**, 1768 (2001).
[23] A. Celani, A. Mazzino, and M. Vergassola, Thermal plume turbulence, Phys. Fluids **13**, 2133 (2001).
[24] A. Celani, T. Matsumoto, A. Mazzino, and M. Vergassola, Scaling and Universality in Turbulent Convection, Phys. Rev. Lett. **88**, 054503 (2002).
[25] T. Gotoh and T. Watanabe, Power and Non-Power Laws of Passive Scalar Moments Convected by Isotropic Turbulence, Phys. Rev. Lett. **115**, 114502 (2015).
[26] R. H. Kraichnan, Turbulent cascade and intermittency growth, Proc. R. Soc. London A **434**, 65 (1991).
[27] T. Gotoh and T. Nakano, Role of pressure in turbulence, J. Stat. Phys. **113**, 855 (2003).
[28] K. Yoshida and Y. Kaneda, Anomalous scaling of anisotropy of second-order moments in a model of a randomly advected solenoidal vector field, Phys. Rev. E **63**, 016308 (2000).
[29] K. Ohkitani, Numerical study of comparison of vorticity and passive vectors in turbulence and inviscid flows, Phys. Rev. E **65**, 046304 (2002).
[30] R. Benzi, L. Biferale, and F. Toschi, Universality in passively advected hydrodynamic fields: The case of a passive vector with pressure, Eur. Phys. J. B **24**, 125 (2001).
[31] E. S. C. Ching, Y. Cohen, T. Gilbert, and I. Procaccia, Active and passive fields in turbulent transport: The role of statistically preserved structures, Phys. Rev. E **67**, 016304 (2003).
[32] N. V. Antonov, M. Hnatich, J. Honkonen, and M. Jurčišin, Turbulence with pressure: Anomalous scaling of a passive vector field, Phys. Rev. E **68**, 046306 (2003).
[33] N. V. Antonov and N. M. Gulitskiy, Anisotropic turbulent advection of a passive vector field: Effects of the finite correlation time, EPJ Web Conf. **108**, 02008 (2016).
[34] H. Arponen, Steady-state existence of passive vector fields under the Kraichnan model, Phys. Rev. E **81**, 036325 (2010).
[35] J. Yang, T. Gotoh, and H. Miura, Intermittency of incompressible passive vector convected by isotropic turbulence (unpublished).
[36] J. R. Herring and R. B. Kerr, Comparison of direct numerical simulations with predictions of two-point closures for isotropic turbulence convecting a passive scalar, J. Fluid Mech. **118**, 205 (1982).
[37] T. Gotoh, D. Fukayama, and T. Nakano, Velocity field statistics in homogeneous steady turbulence obtained using a high-resolution direct numerical simulation, Phys. Fluids **14**, 1065 (2002).
[38] D. A. Donzis and K. R. Sreenivasan, The bottleneck effect and the Kolmogorov constant in isotropic turbulence, J. Fluid Mech. **657**, 171 (2010).
[39] Y. Kaneda, T. Ishihara, M. Yokokawa, K. Itakura, and A. Uno, Energy dissipation rate and energy spectrum in high resolution direct numerical simulations of turbulence in a periodic box, Phys. Fluids **15**, L21 (2003).
[40] T. Gotoh and D. Fukayama, Pressure Spectrum in Homogeneous Turbulence, Phys. Rev. Lett. **86**, 3775 (2001).
[41] Y. Tsuji and Y. Kaneda, Anisotropic pressure correlation spectra in turbulent shear flow, J. Fluid Mech. **694**, 50 (2012).
[42] K. R. Sreenivasan, On local isotropy of passive scalars in turbulent shear flows, Proc. R. Soc. London A **434**, 165 (1991).
[43] A. Pumir, A numerical study of the mixing of a passive scalar in three dimensions in the presence of a mean gradient, Phys. Fluids **6**, 2118 (1994).
[44] M. Holzer and E. D. Siggia, Turbulent mixing of a passive scalar, Phys. Fluids **6**, 1820 (1994).
[45] K. R. Sreenivasan, R. A. Antonia, and D. Britz, Local isotropy and large structures in a heated turbulent jet, J. Fluid Mech. **94**, 745 (1979).

[46] M. R. Overholt and S. B. Pope, Direct numerical simulation of a passive scalar with imposed mean gradient in isotropic turbulence, Phys. Fluids **8**, 3128 (1996).
[47] G. Falkovich, Bottleneck phenomenon in developed turbulence, Phys. Fluids **6**, 1411 (1994).
[48] Y. Kaneda, Renormalized expansions in the theory of turbulence with the use of the Lagrangian position function, J. Fluid Mech. **107**, 131 (1981).
[49] Y. Kaneda, Inertial range structure of turbulent velocity and scalar fields in a Lagrangian renormalized approximation, Phys. Fluids **29**, 701 (1986).
[50] T. Gotoh, Passive scalar diffusion in two dimensional turbulence in the Lagrangian renormalized approximation, J. Phys. Soc. Jpn. **58**, 2365 (1989).
[51] T. Gotoh and T. Watanabe, Statistics of transfer fluxes of the kinetic energy and scalar variance, J. Turbul. **6**, 33 (2005).
[52] P. D. Mininni, A. Alexakis, and A. Pouquet, Nonlocal interactions in hydrodynamics turbulence at high Reynolds numbers: The slow emergence of scaling laws, Phys. Rev. E **77**, 036306 (2008).
[53] T. Gotoh, Y. Watanabe, Y. Shiga, T. Nakano, and E. Suzuki, Statistical properties of four-dimensional turbulence, Phys. Rev. E **75**, 016310 (2007).